Scientific African 28 (2025) e02652

Contents lists available at ScienceDirect

Scientific African

journal homepage: www.elsevier.com/locate/sciaf

Hemodynamic properties of blood flow in an angled overlying stenosed blood vessel via force field and gold nanoparticle suspension

M. Dhange [a,b,*], S. Salgare [b,c], Kusal K. Das [d], Ebenezer Bonyah [e], Habtu Alemayehu [f]

[a] Department of Mathematics, BLDEA's VP Dr. PG Halakatti College of Engineering and Technology, Vijayapur, 586103, India
[b] Visvesvaraya Technological University, Belagavi, Karnataka, India
[c] Department of Mathematics, Sanjay Ghodawat University, Kolhapur, Maharashtra, India
[d] Department of Physiology, Laboratory of Vascular Physiology and Medicine, Shri B.M. Patil Medical College, Hospital and Research Centre, BLDE (Deemed to be University), Vijayapur, India
[e] Department of Mathematics Education, Akenten Appiah Menka University of Skills Training and Entrepreneurial Development, Kumasi, Ghana
[f] Department of Mathematics, College of Natural and Computational Sciences, Mekelle University, Tigary, Ethiopia

ARTICLE INFO

Editor: DR B Gyampoh

Keywords:
Flow resistivity (FR)
Gold nanoparticles
Inclined artery
Magnetic field
Overlying stenosis
Wall shear stress (WSS)

JEL classification:
76Z05
92C10

ABSTRACT

A review of the literature on nanoparticles indicates that the use of nanofluids in hematological treatments is growing. This effort presents a theoretical investigation of the non-linear behavior of blood flow mixed with suspensions of gold nanoparticles (Au-NP's) in the presence of a force field and water is used as base fluid in an angled arterial section with overlying stenosis. An elastic cylindrical tube with a moving wall is used to represent the artery, and a viscous liquid is used to simulate the blood flowing through it. The geometry of an overlying segment of a stenosed artery can be quantitatively represented by a valid geometric expression. The coupled partial differential equations are used to formulate blood rheology theoretically. The current analytical method can compute the wall shear stress (WSS), flow resistivity (FR), temperature, and velocity profiles with mild stenosis assumption by applying the boundary conditions. Numerical calculations of the desired quantities are carried out systematically. The results are graphically presented in the discussion section. They provide an overview of how the degree of stenosis with gold nanoparticles and the malleability of the artery wall influence blood flow abnormalities. This shows that gold-NPs can enhance hemodynamic performance and improve blood flow in stenosed blood arteries. Together with an increase in the proclivity angle, the surface shear stress and the resistivity to flow both rise with the height of stenosis. The results obtained from this study may help medical practitioners to predict the flow behavior in diseased arteries.

Introduction

One of the disorders influencing our human cardiovascular system is blood arterial constriction brought on by aberrant tissue growth. Lifeblood flow may be reduced or impeded as a result, potentially leading to serious cardiovascular disorders. One of the main causes of death in affluent nations nowadays is cardiac illness. The cardiovascular disease framework, which is collectively made up of

* Corresponding author.
E-mail address: math.mallinath@bldeacet.ac.in (M. Dhange).

https://doi.org/10.1016/j.sciaf.2025.e02652
Received 15 December 2024; Received in revised form 22 February 2025; Accepted 17 March 2025
Available online 18 March 2025

Nomenclature

L	length of the tube (m)
L_0	length of stenosis (m)
d	Beginning of the stenosis region
δ	maximum height of stenosis (m)
w	Velocity of fluid (m/s)
z	axial coordinate (m)
r	radial coordinate (m)
θ	angle of proclivity $(radian)$
$R(z)$	radius of the artery (m)
R_0	the radius of the normal artery (m)
p	pressure across the region (kg/ms^2)
h	length of the geometry of overlapping stenosed artery wall (m)
$\overline{\lambda}$	resistance to the flow (kg/m^4s)
$\overline{\tau}_w$	wall shear stress (N/m^2)
$(T,\ \Theta)$	temperature $(Kelvin\ (K))$
μ	blood viscosity (kg/ms)
$M,\ B_0$	Forced field or magnetic field $(tesla\ (T))$
Q_0	Heat-generating or absorbing element (J)
g	acceleration due to gravity (m/s^2)
C	Average velocity over the radius R_0 of the tube (m/s)
β	Hear absorbing constraint
G_r	Grashof number
μ_{nf}	Dynamic viscosity of nano-fluid (kg/ms)
ρ_{nf}	density nano-fluid (kg/m^3)
α_{nf}	thermal diffusivity nano-fluid (m^2/s)
k_{nf}	thermal conductivity nano-fluid (W/mK)
$(\rho c_p)_{nf}$	heat capacitance nano-fluid (J/K)
q	volume flow rate (kW/m^2)
ρ	the density of the fluid (kg/m^3)
σ	electrical conductivity
(w, v)	Velocity components in $(r,\ z)$ direction respectively (m/s)

blood vessels and the heart, allows blood to circulate through them. The way blood flows can be dramatically altered by vascular disorders. Nowadays, lifeblood vessels and heart diseases, including heart attacks and strokes, pose major health risks and account for a large percentage of deaths. These disorders are closely linked to the features of lifeblood flow and vascular behavior. The primary cause of these deaths is stenosis. The construction of an artery due to the formation of arteriosclerotic lesions or another type of aberrant tissue growth is referred to as "stenosis". Although the precise reasons for stenosis are still unknown, it has been proposed that deposits of cellular waste products, saturated fat, and fatty material on the artery wall are the culprits. Blood flow is reduced when stenosis develops in an artery. When stenosis occurs in an artery, it can cause damage that affects the circulatory system's normal function. In particular, it may result in heart attacks. Restricting blood flow can damage the wall's inner cells and accelerate the development of stenosis. Because one influences the other, there is a connection between the artery's lifeblood flow and the development of stenosis. The impression of stenosis on the continuous flow of lifeblood via a conduit was initially examined by Young [1]. Azuma-Fukushima [2] developed simulations of patterns of circulation in stenosed blood vessel walls. Vascular stenosis's impact on constant flow was observed by MacDonald [3]. The flow features of lifeblood in a pipe with minor contraction were then examined in a variety of research using lifeblood under different circumstances, such as non-Newtonian or Newtonian fluids (see [4–12]).

Chakraborty-Mandal [13,14] examined the blood flow in overlaying stenosis with body spurt using a mathematical model. The impact of the 2-layered non-Newtonian stream and overlying stenosis on arterial flow has been studied by Srivastava et al. [15,16]. Riahi et al. [17] looked at the arterial stream in the setting of overlying stenosis. The mathematical representation of irregular blood circulation in viscoelastic tapering arteries with overlaying stenosis was examined by Haghighi et al. [18]. Subsequent research examined the impact of overlapping stenosis on blood flow via different arterial configurations (see to [19–23]).

A uniform blend of nanoparticles (NPs) derived from a base fluid is recognized as a nanofluid (NF). Carbides, oxides, metals, and carbon nanotubes make up the nanoparticles. Ethylene glycol, water, and oil make up a base fluid. Chio [24] was the first to suggest the nanofluid. The thermophysical properties of nanofluids may be superior to those of traditional fluids. Nanofluids are used in a wide range of heat-transfer-related industries, namely fuel-cell technology, microelectronics, hybrid power engines, medications, refrigeration equipment, home fridges, nuclear reactor coolants, and space technologies. Several researchers [25–35] discussed the mixed

Table 1
Thermophysical characteristics of blood, water, and gold nanoparticles (Au) (Pak and Cho [52]).

Physical properties	Gold	Blood	Fluid phase
$\rho\ (kg/m\hat{}3)$	19,320	1063	997.1
$c\_p\ (J/kg\,K)$	128.8	3594	4179
$K(W/m\,K)$	314.4	0.492	0.613
$\gamma\, x\, 10^{-5}\ (K^{-1})$	1.4×10^{-5}	0.18	21.0

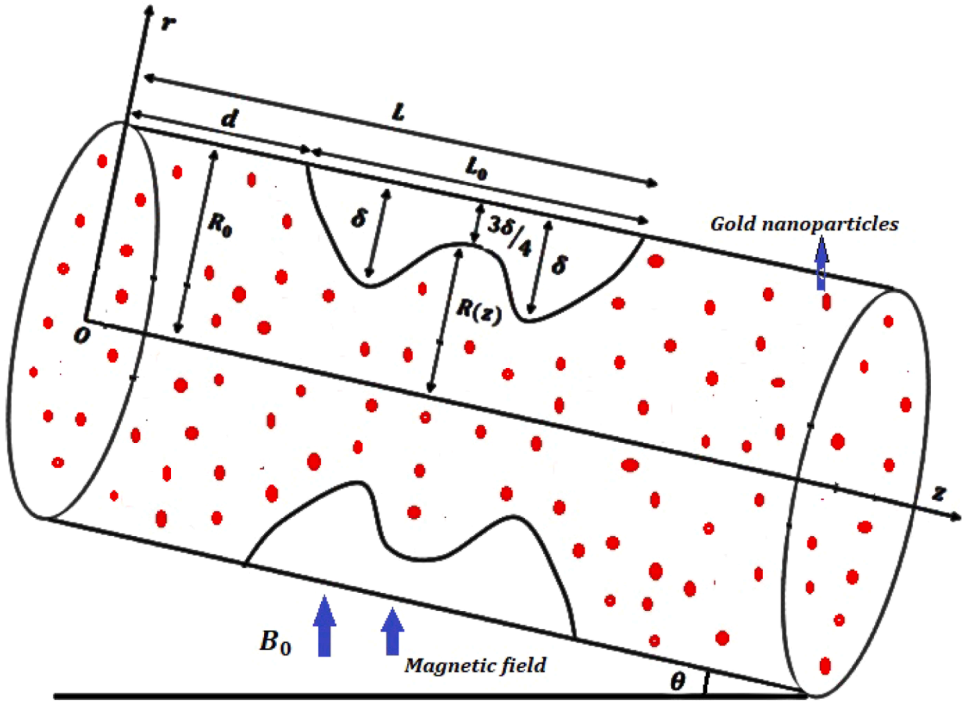

Fig. 1. Design of overlying stenosis.

blood flow of nanoparticles and showed that this approach allows us to predict such issues and get the right results.

Vajravelu et al. [36] focused on Ag-water and Cu-water nanofluids (NFs) and examined convective thermal transfer in a nanofluid (NF) stream that terminates in an elongating surface. They examined the properties of the NPs capacity element on the stream in addition to the high-temperature uniqueness under the infection-dependent generation of internal heat or integration and thermal resilience capabilities. The effects of thermal energy generation and flow in the peristalsis with tiny particles contacting H2O+Cu were thoroughly elucidated by Akbar et al. [37].

They contrasted the outcomes for copper-water (Cu-water) with the pure-water foundation model. Akbar [38] looked into how endoscopes affected the peristaltic stream of a Cu-water nanofluid (NF). In a work by Akbar et al. [39], the effects of copper tiny fluids on wall characteristics and a curve-shaped conduit with peristalsis were investigated. Elnaqeen et al. [40] investigated the Cu-blood stream model using a catheterized mild stenotic artery with thrombosis. Along with copper and silver nanoparticles, researchers Zaman et al. [41] examined the impact of slip-on unstable blood flow over a curved stenosed channel. In a separate study, Zaman et al. [42] examined the volatile scattering of nanoparticles in blood. The paper describes the non-Newtonian features of blood using the Carreau liquid model. Elnaqeeb et al. [43] inspected the hemodynamic features of a stream of blood including gold nanoparticles in a shortened artery through flexible viscosity. The combined investigation by Mekheimer et al. [44] investigated the effects of magnetic forces and metallic nanoparticles on a micropolar fluid passing through an overlying stenotic artery. Studies on further applications of nanoparticles (NPS) in blood physiology carried out by different researchers are included in the references [45–50].

Arterial stenosis can lead to serious issues and interfere with the heart's and lungs' regular functions. In particular, it may lead to: a spike in flow resistance that may cause a substantial decrease in blood flow; an increased risk of complete occlusion; and abnormal growth of cells in the stenotic area. However, several researchers have used suspended nanoparticles to study the effects of various types of stenosis on arterial blood flow [51–60]. Table 1 displays the thermophysical characteristics of gold nanoparticles (NPs), water, and blood.

Inspired by the previous research, the current work uses water as the basic fluid and gold nanoparticles to examine the special effects of a force field on lifeblood flow. This liquid appears to travel through a sloping, overlying stenosed artery (Fig. 1). We analyze

the pressure droplet, flow resistance, and shear stress at the wall, and the figures show the distinct effects of several important limitations. Section 2 provides a detailed explanation of the mathematical and physical models. The results obtained are then discussed in Section 3.

Formulation of the problem and its solution

Examine the movement of a sticky incompressible liquid via a tube that has an angled axisymmetric overlap and a uniform cross-section. In the axial direction, the stenosis should grow symmetrically and be mild. The surface shape is shown in Fig. 1.

The mathematical equation is (Chakraborty-Mandal [13], Srivastava et al. [15]) for the stenosed surface.

$$h=\frac{R(z)}{R_0}=\begin{cases}1-\dfrac{3\delta}{2R_0L_0^4}\left[11(z-d)L_0^3-47(z-d)^2L_0^2+72(z-d)^3L_0-36(z-d)^4\right]:d\le z\le d+L_0\\ \\ 1:\textit{otherwise}\ .\end{cases} \tag{1}$$

In this case, the artery's normal segment radius is R_0, the tube's radius at the stenotic area is $R(z)$, the stenotic area begins at position d, and the tube's length is L. The proclivity angle is θ, and the length of the stenotic region is measured by L_0. The length of overlapping stenosis is h, and the maximum height of the stenosis, as measured from the origin, is δ at $z=d+L_0/6$, $z=d+5L_0/6$, and the critical height at $z=d+\frac{L_0}{2}$ is $\frac{3\delta}{4}$.

Leading mathematical formula

This understanding states that lifeblood is a non-Newtonian, consistent, and incompressible liquid. A variety of non-Newtonian liquid prototypes, such as the power-law, micropolar, Herschel-Bulkley, and other liquid structures, can be used to characterize its viscosity. We adopted the viscous liquid paradigmatic to describe the physical stuff of blood in our work because, in comparison to other viscidness prototypes, it accurately depicts the viscosity characteristic of physiological blood in everyday life (Pratumwal et al. [55]).

The following is a crucial articulation of the flow for the current situation, as per Akbar-Butt [48]:

$$\frac{\partial v}{\partial r}+\frac{v}{r}+\frac{\partial w}{\partial z}=0, \tag{2}$$

$$\rho_{nf}\left(v\frac{\partial v}{\partial r}+w\frac{\partial v}{\partial z}\right)=-\frac{\partial p}{\partial r}+\mu_{nf}\frac{\partial}{\partial r}\left(2\frac{\partial v}{\partial r}\right)+\mu_{nf}\frac{\partial}{\partial z}\left(2\frac{\partial v}{\partial z}+\frac{\partial w}{\partial r}\right)-\rho_{nf}\mathrm{g}\cos\theta, \tag{3}$$

$$\rho_{nf}\left(v\frac{\partial w}{\partial r}+w\frac{\partial w}{\partial z}\right)=-\frac{\partial p}{\partial z}+\mu_{nf}\frac{\partial}{\partial z}\left(2\frac{\partial w}{\partial z}\right)+\frac{\mu_{nf}}{r}\frac{\partial}{\partial r}\left[r\left(\frac{\partial v}{\partial z}+\frac{\partial w}{\partial r}\right)\right]-g\rho_{nf}\alpha(T-T_0)-\sigma B_0^2w+\rho_{nf}\mathrm{g}\sin\theta, \tag{4}$$

$$\left(v\frac{\partial T}{\partial r}+w\frac{\partial T}{\partial z}\right)=\frac{K_{nf}}{(\rho c_p)_{nf}}\left(\frac{\partial^2T}{\partial r^2}+\frac{1}{r}\frac{\partial T}{\partial r}+\frac{\partial^2T}{\partial z^2}\right)+\frac{Q_0}{(\rho c_p)_{nf}}. \tag{5}$$

Theoretical solution and borderline conditions (BC)

In order to calculate the solutions to mimicked physical problems, boundary restrictions are crucial. It may be deduced that the axial speed (w) of the lifeblood components on the surface corresponds to a one-dimensional stream and is the same as the rapidness of arterial membrane stuff since lifeblood elements adhere to the interior surface of the artery piece under consideration.

The stenosed element of this can be quantitatively described as follows:

$$\frac{\partial w}{\partial r}=0,\ \frac{\partial T}{\partial r}=0\ at\ r=0, \tag{6}$$

$$w=0,\ T=0\ at\ r=h. \tag{7}$$

The hotness of the fluid is denoted by T, the heat-generating or heat-absorbing element by Q_0, and the rapidity components in the $(r,\ z)$ directions by $(w,\ v)$ respectively.

The following are the specified values for the nanofluids' active dynamic viscosity $\left(\mu_{nf}\right)$, active density $\left(\rho_{nf}\right)$, active thermal conductivity $\left(k_{nf}\right)$, thermal diffusivity $\left(\alpha_{nf}\right)$, and heat capacitance $\left(\rho c_p\right)_{nf}$, respectively (see [36,43]):

$$\mu_{nf}=\frac{\mu_f}{(1-\varphi)^{2.5}},\ \rho_{nf}=(1-\varphi)\rho_f+\varphi\rho_f,\ k_{nf}=\ k_f\left\{\frac{k_s+2k_f-2\ \varphi\left(k_f-k_s\right)}{k_s+2k_f+2\varphi\left(k_f-k_s\right)}\right\},$$

$$\alpha_{nf} = \frac{k_{nf}}{(\rho c_p)_{nf}},\ (\rho c_p)_{nf} = (1-\varphi)(\rho c_p)_f + \varphi(\rho c_p)_f .$$

The dimensionless amounts used were as follows:

$$\begin{aligned} &\bar{r} = \frac{r}{R_0},\ \bar{z} = \frac{z}{L_0},\ \bar{w} = \frac{w}{W},\ \bar{v} = \frac{L_0}{\delta W}v,\ \bar{d} = \frac{d}{L_0},\ \bar{R} = \frac{R}{R_0},\ \bar{p} = \frac{WL_0\mu}{R_0^2}p \\ &M^2 = \frac{\sigma B_0^2 R_0^2}{\mu_f},\ G_r = \frac{g\alpha R_0^2 T_0 \rho_{nf}}{W\mu_f},\ F = \frac{\mu_{nf} c}{\rho_{nf} g R_0^2},\ \bar{\delta} = \frac{\delta}{R_0},\ \Theta = \frac{T-T_0}{T_0},\ \beta = \frac{Q_0 R_0^2}{k_f T_0} \end{aligned} \tag{8}$$

In this case, c is the average velocity over the radius R_0 of the tube section.

After removing the dashes, we obtain the following when we apply the aforementioned scaling variables of Eq. (8) in Eqs. (2)–(5) and moderate stenosis $\left(\frac{\delta}{R_0} \ll 1\right)$ condition $\epsilon = \frac{R_0}{L_0} = o(1)$.

$$\frac{\partial \mathrm{p}}{\partial \mathrm{r}} = -\frac{\cos\theta}{F}, \tag{9}$$

$$\frac{\mathrm{dp}}{\mathrm{dz}} = \frac{1}{(1-\varphi)^{2.5}}\frac{1}{r}\frac{\partial}{\partial r}\left(r\frac{\partial \mathrm{w}}{\partial \mathrm{r}}\right) - M^2 w + G_r\Theta + \frac{\sin\theta}{F}, \tag{10}$$

$$\frac{1}{r}\frac{\partial}{\partial r}\left(r\frac{\partial \Theta}{\partial \mathrm{r}}\right) + \beta\left(\frac{k_{nf}}{k_f}\right) = 0. \tag{11}$$

The following are the required temperature and velocity boundary circumstances for the artery wall using scaling variables:

$$\frac{\partial w}{\partial r} = 0,\ \frac{\partial \Theta}{\partial r} = 0 \text{ at } r = 0, \tag{12}$$

$$w = 0,\ \Theta = 0 \text{ at } r = h. \tag{13}$$

where Θ is the temperature, M is the forced field constraint, β is the amount of heat absorbing constraint, and G_r is the Grashof number.

The fluid's velocity is computed as follows by taking into consideration the constraint for moderate stenosis and handling Eq. (10) and Eq. (11) inside the boundary limitation Eqs. (12) and (13):

$$w = \left\{\frac{\frac{1}{M^2}\frac{dp}{dz} - \frac{G_r\beta}{M^2}\left(\frac{k_f}{k_{nf}}\right) - \frac{1}{M^2}\frac{Sin\ \theta}{F}}{I_0\left(Mh\sqrt{(1-\varphi)^{2.5}}\right)}\right\} I_0\left(Mr\sqrt{(1-\varphi)^{2.5}}\right) - \frac{G_r\beta}{4M^2}\left(\frac{k_f}{k_{nf}}\right)(r^2-h^2) - \frac{1}{M^2}\frac{dp}{dz} + \frac{G_r\beta}{M^2}\left(\frac{k_f}{k_{nf}}\right) - \frac{1}{M^2}\frac{Sin\ \theta}{F}, \tag{14}$$

$$\Theta = \frac{-\beta}{4}\left(\frac{k_f}{k_{nf}}\right)(r^2-h^2). \tag{15}$$

The flow rate q is as follows (see [48,54]):

$$q = 2\int_0^h rw dr. \tag{16}$$

This provides us with:

$$\frac{dp}{dz} = \frac{q - \frac{G_r\beta h^4}{16M^2}\left(\frac{k_f}{k_{nf}}\right) - \frac{G_r\beta h^2}{2M^2}\left(\frac{k_f}{k_{nf}}\right) + \frac{G_r\beta h}{M^2}\left(\frac{k_f}{k_{nf}}\right)\left(\frac{I_1\left(Mh\sqrt{(1-\varphi)^{2.5}}\right)}{I_0\left(Mh\sqrt{(1-\varphi)^{2.5}}\right)\sqrt{(1-\varphi)^{2.5}}}\right) + \frac{h}{M^2}\frac{Sin\ \theta}{F}\left(\frac{I_1\left(Mh\sqrt{(1-\varphi)^{2.5}}\right)}{I_0\left(Mh\sqrt{(1-\varphi)^{2.5}}\right)\sqrt{(1-\varphi)^{2.5}}}\right) + \frac{h^2}{M^2}\frac{Sin\ \theta}{F}}{\frac{-h^2}{2M^2} + \frac{h}{M^3}\left(\frac{I_1\left(Mh\sqrt{(1-\varphi)^{2.5}}\right)}{I_0\left(Mh\sqrt{(1-\varphi)^{2.5}}\right)\sqrt{(1-\varphi)^{2.5}}}\right)} \tag{17}$$

The pressure decreases across a single wavelength, $p(0) - p(\lambda)$, is given by the following formula:

$$\Delta p = -\int_0^1 \frac{dp}{dz}\, dz. \tag{18}$$

The following is a description of the impedance, denoted by λ:

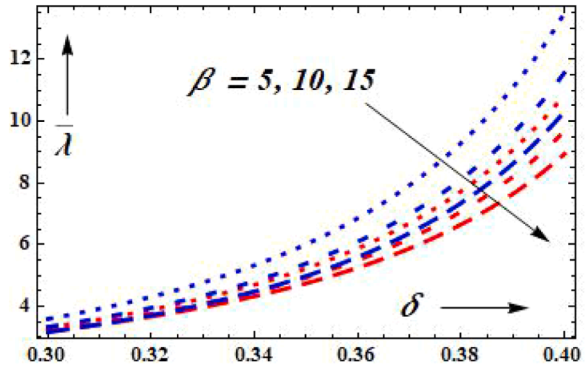

Fig. 2. Design of $\bar{\lambda}$ for β through $\theta = \pi/6,\ q = 1.0,\ G_r = 3.0,\ M = 2.5,\ d = 0.2,\ L_0 = 0.4,\ F = 0.8,\ L = 1.$

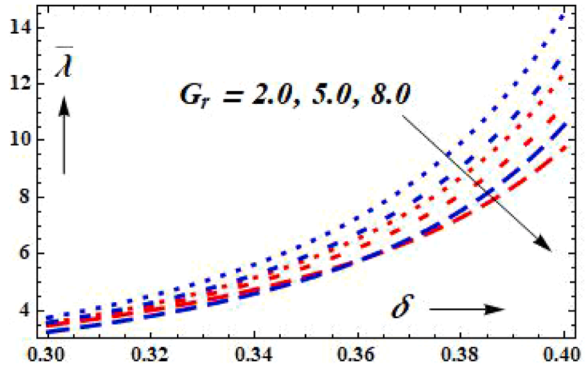

Fig. 3. Design of $\bar{\lambda}$ for G_r through $\theta = \pi/6,\ q = 1.0,\ \beta = 6.0,\ M = 2.0,\ d = 0.2,\ L_0 = 0.4,\ F = 0.8,\ L = 1.$

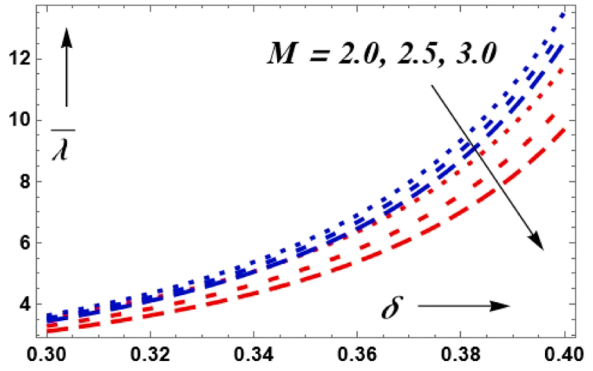

Fig. 4. Design of $\bar{\lambda}$ for M through $\theta = \pi/6,\ q = 1.0,\ \beta = 6.0,\ G_r = 3.0,\ d = 0.2,\ L_0 = 0.4,\ F = 0.8,\ L = 1.$

$$\lambda = \frac{\Delta p}{q}. \tag{19}$$

Since stricture is absent $(h = 1)$, the following deliberate pressure reduction is carried out:

$$\Delta p_n = \left[-\int_0^1 \frac{dp}{dz}\, dz \right]_{h=1.} \tag{20}$$

The flow resistivity quickly influences the bloodstream rate and has a direct effect on the bloodstream. The subsequent method can be used to determine the impedance in a normal artery:

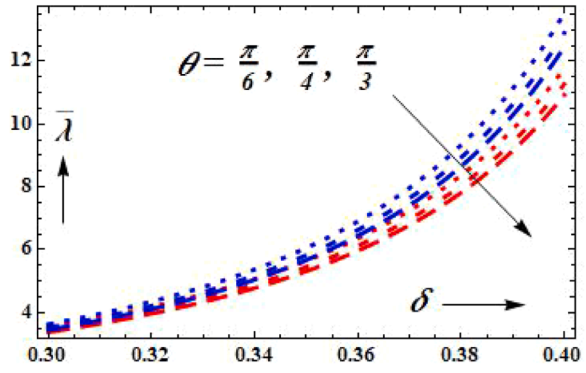

Fig. 5. Design of $\bar{\lambda}$ for θ through $M = 2.0,\ q = 1.0,\ \beta = 6.0,\ G_r = 3.0,\ d = 0.2,\ L_0 = 0.4,\ F = 0.8,\ L = 1$.

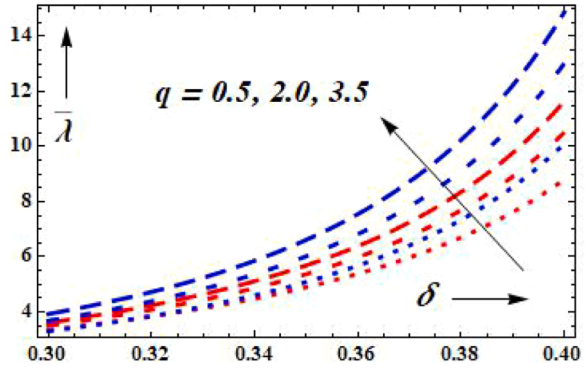

Fig. 6. Design of $\bar{\lambda}$ for q through $M = 2.0,\ \theta = \pi/6,\ \beta = 12,0,\ G_r = 3.0,\ d = 0.2,\ L_0 = 0.4,\ F = 0.8,\ L = 1$.

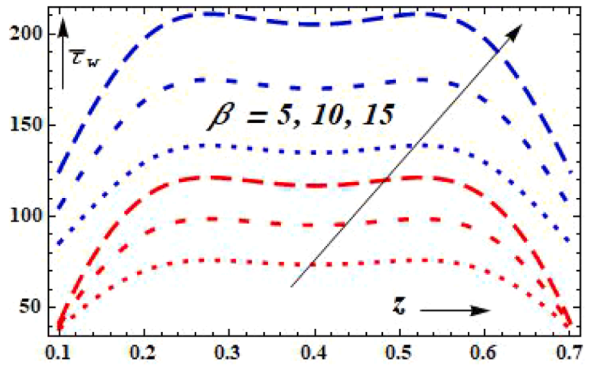

Fig. 7. Design of $\bar{\tau}_h$ for β through $\delta = 0.03,\ \theta = \pi/6,\ q = 1.0,\ G_r = 3.0,\ M = 2.0,\ d = 0.2,\ L_0 = 0.4,\ F = 0.8,\ L = 1$.

$$\lambda_n = \frac{\Delta p_n}{q}\ . \tag{21}$$

A stream's normalized resistance is expressed as follows:

$$\bar{\lambda} = \frac{\lambda}{\lambda_n}\ . \tag{22}$$

One of the physical elements that significantly affects the fluid flow at the blood artery wall is the shear stress in the wall. The wall shear stress can be computed using the formula below:

$$\bar{\tau}_w = -\frac{h}{2}\frac{dp}{dz}\ . \tag{23}$$

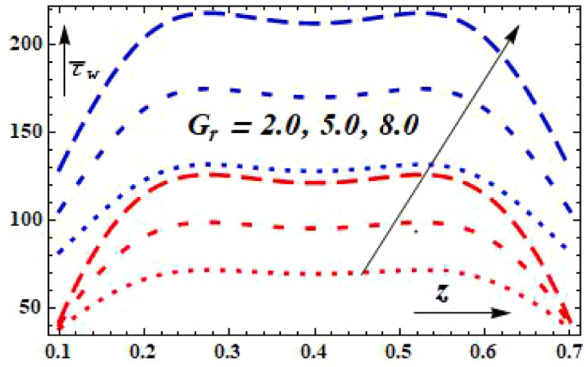

Fig. 8. Design of $\overline{\tau}_h$ for G_r through $\theta = \pi/6$, $q = 1.0$, $\beta = 6.0$, $M = 2.0$, $d = 0.2$, $L_0 = 0.4$, $F = 0.8$, $\delta = 0.03$, $L = 1$.

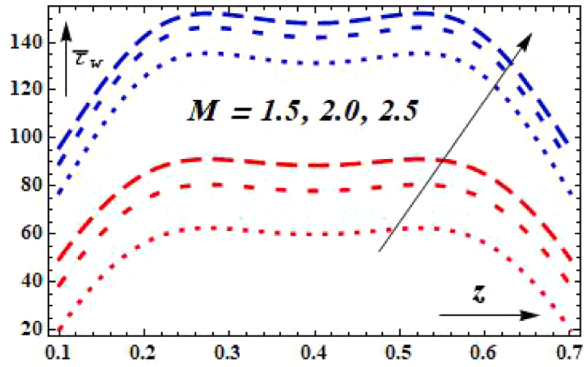

Fig. 9. Design of $\overline{\tau}_h$ for M through $\theta = \pi/6$, $q = 1.0$, $\beta = 6.0$, $G_r = 3.0$, $d = 0.2$, $L_0 = 0.4$, $\delta = 0.03$, $F = 0.8$, $L = 1$.

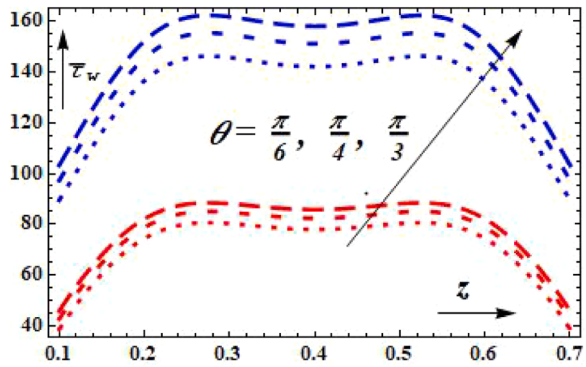

Fig. 10. Design of $\overline{\tau}_h$ for θ through $\delta = 0.03$, $M = 2.0$, $q = 1.0$, $\beta = 6.0$, $G_r = 3.0$, $d = 0.2$, $L_0 = 0.4$, $F = 0.8$, $L = 1$.

Computational results and discussion

In this research, appropriate numerical computation has been presented to test the validity of the analytical expressions Eqs. (14, 15, 22, 23). The effects of various constraints were examined using MATHEMATICA software. Figs. 2–19 display the entire set of findings. In figures, the color blue ($\varphi \neq 0$) represents Au-blood, whereas the color red ($\varphi = 0$) represents pure blood.

Figs. 2–6 illustrate the relationship between flow resistance(FR) and stenosis height for different values of the heat absorption constant (β), Grashof number (G_r), force field constraint (M), angle of proclivity (θ), and flow rate (q). It is clear that the FR rises in tandem with the stenosis height (δ) for all constraints. However, according to Fig. 2, it decreases with the heat absorption constant (β). It is important to note the physical basis for this observation. For a brief time, the fluid increases flow resistance in the pre-stenotic zone before reaching its minimum in the post-stenotic region because the obstructed fluid in the constriction region swiftly travels towards the main flow region. Moreover, it is seen that while flow impedance increases with an increase in volume flow rate (see Fig. 6), FR

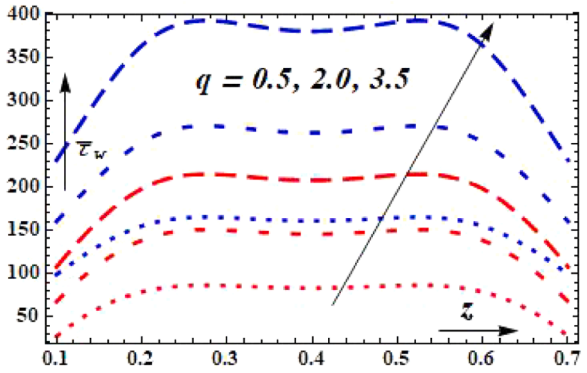

Fig. 11. Design of $\overline{\tau}_h$ for q through $\theta = \pi/6$, $M = 2.0$, $\beta = 12.0$, $\delta = 0.03$, $G_r = 3.0$, $d = 0.2$, $L_0 = 0.4$, $F = 0.8$, $L = 1$.

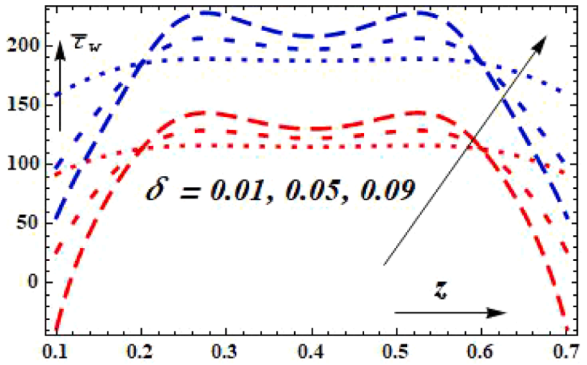

Fig. 12. Design of $\overline{\tau}_h$ for δ through $\theta = \pi/6$, $M = 2.5$, $\beta = 12.0$, $G_r = 3.0$, $d = 0.2$, $L_0 = 0.4$, $F = 0.8$, $L = 1$.

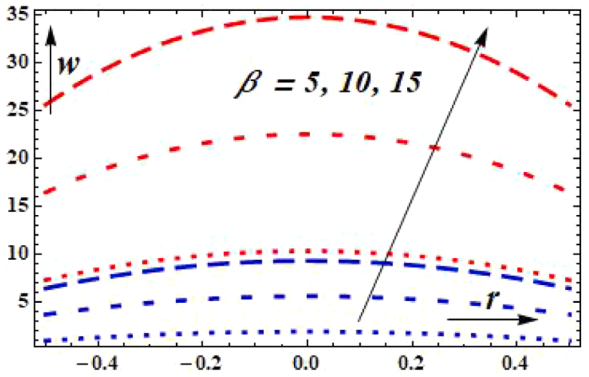

Fig. 13. Design of w for β through $\theta = \pi/6$, $M = 1.5$, $G_r = 3.0$, $d = 0.2$, $L_0 = 0.4$, $z = 0.5$, $\delta = 0.03$, $F = 0.8$, $L = 1$.

reduces with increases in the Grashof number (G_r), force field constraint (M), flow rate (q), and angle of proclivity (θ) (see Figs. 3-6). Blood can flow through arteries with ease when there is a drop in flow resistance due to a rise in fluid velocity caused by an increase in volume flow rate, angle of inclination, and high buoyancy forces. Further, it is found that Au-blood has more reluctance to flow than pure blood. This is because gold makes arteries more flexible. These results concur with those of Elnaqeeb [54].

Figs. 7-12 demonstrate the wall shear stress(WSS) $(\overline{\tau}_w)$ against the axial distance (z) for various values of the Grashof number (G_r), stenosis height (δ), heat absorption constant (β), angle of proclivity (θ), force field constraint (M), and flow rate (q). It is found that the Grashof number (G_r), the force field constraint (M), and the heat absorption constant all raise the WSS$(\overline{\tau}_w)$. Compared to pure blood, this fluctuation is more pronounced when Au particles are present in the blood. Additionally, it is examined that. $\overline{\tau}_w$ rises as the flow rate (q) and angle of proclivity (θ) grow. The WSS is observed to grow from $z = 0.1$ to 0.25, then fall to $z = 0.4$, then climb once more to $z = 0.53$, before progressively declining and approaching 0.7. This illustrates that the WSS is greatest at the throats and lowest at the critical height of the stenosis. These results align with the findings of [45,54].

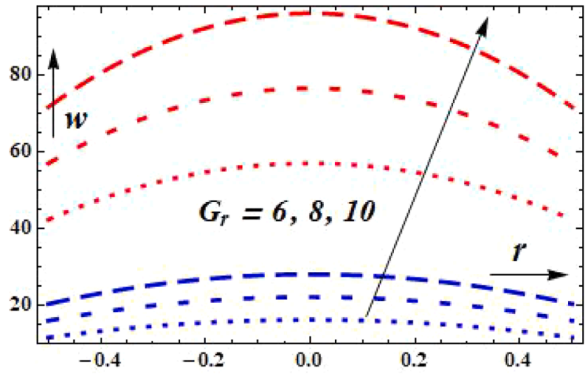

Fig. 14. Design of w for G_r through $\theta = \pi/6$, $M = 1.5$, $\beta = 12.0$, $d = 0.2$, $L_0 = 0.4$, $F = 0.8$, $z = 0.5$, $\delta = 0.03$, $L = 1$.

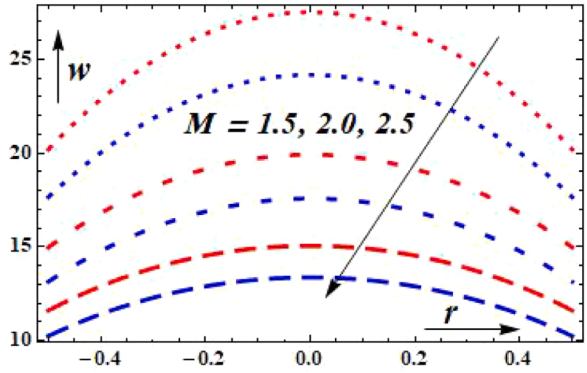

Fig. 15. Design of w for M through $\theta = \pi/6$, $G_r = 3.0$, $\beta = 12.0$, $z = 0.5$, $\delta = 0.03$, $d = 0.2$, $L_0 = 0.4$, $F = 0.8$, $L = 1$.

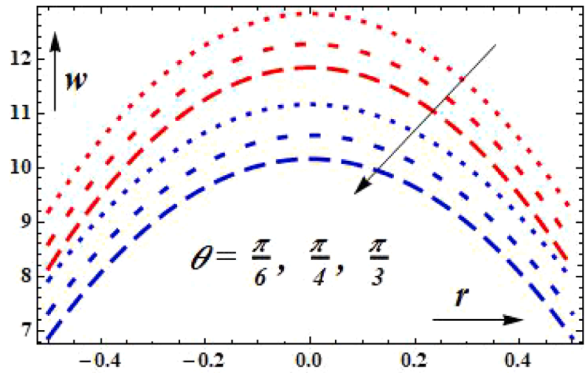

Fig. 16. Design of w for θ through $M = 1.5$, $z = 0.5$, $\delta = 0.03$, $G_r = 3.0$, $\beta = 6.0$, $d = 0.2$, $L_0 = 0.4$, $F = 0.8$, $L = 1$.

Figs. 13–17 show the speed variation across the radial axis for various values of the Grashof number (G_r), force field constraint (M), stenosis height (δ), heat absorption constant (β), and angle of proclivity (θ). Fig. 13 shows that speed rises with an increase in the heat absorption constant (β). As the heat absorption constant rises, the blood becomes thinner than it was before and travels through arteries more quickly, increasing the velocity. Fluid speed rises as the Grashof number (G_r) increases whereas it falls as the force constant (M) Increases (see Figs. 14, 15). Blood can move slowly in arteries when the velocity field is reduced by strong buoyancy and electromagnetic forces relative to viscous forces. Fig. 16 illustrates how increasing the proclivity angle (θ) reduces the fluid's speed. As stenosis height increases, blood flows through arteries more slowly, which lowers speed (Fig. 17). It is also observed that pure blood has a higher velocity than Au-blood because gold causes arteries to become more flexible, which reduces the flow rate. These results coincide with those of Elnaqeeb [54] and Elnaqeeb et al. [43].

Here, Figs. 18, 19 show how temperature (Θ) changes with radial distance (r) for varying values of stenosis height (δ) and a heat

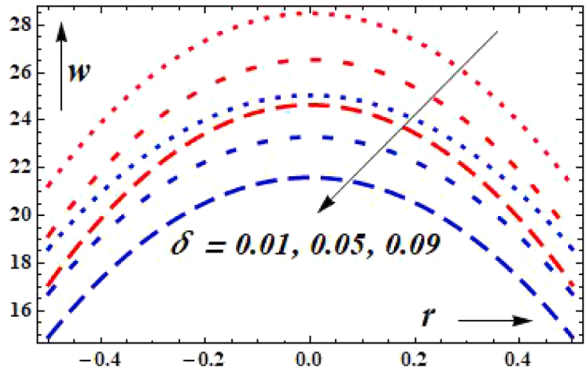

Fig. 17. Design of w for δ through $M = 1.5,\ G_r = 3.0,\ \beta = 12.0,\ d = 0.2,\ L_0 = 0.4,\ F = 0.8,\ z = 0.5,\ L = 1$.

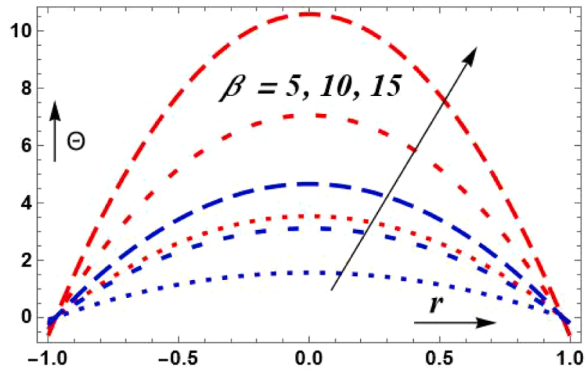

Fig. 18. Design of Θ for β through $z = 0.5,\ \delta = 0.03.\ d = 0.2,\ L_0 = 0.4,\ F = 0.8,\ L = 1$.

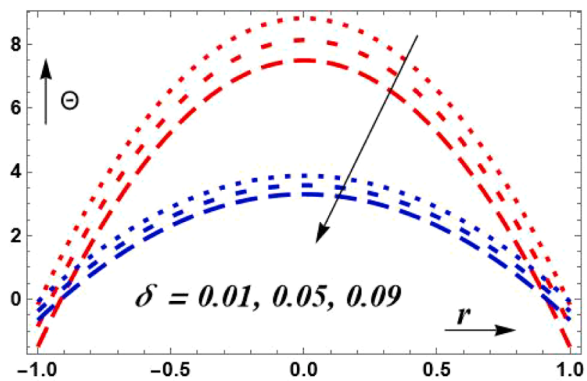

Fig. 19. Design of Θ for δ through $z = 0.5,\ \beta = 12.0.\ d = 0.2,\ L_0 = 0.4,\ F = 0.8,\ L = 1$.

source or sink constraint (β). When the heat absorption constant increases, the temperature rises; however, when the stenosis height increases, the temperature falls. Another finding is that pure blood exhibits a faster temperature change than Au-blood. These findings support Akabar's findings [51].

Concluding observations

The goal of the current mathematical model is to investigate how a forced field affects blood flow through an overlying stenosed passage using water as the base liquid and gold NPs. The results are represented graphically for varied radial distance, inclination angle, stenosis altitude, and expansion following stenosis values. The main conclusions are as follows:

1. As the volume flow rate (q) grows, the flow resistance rises, but as the heat absorption constraint (β), proclivity angle (θ), Grashof number (G_r), and force field constraint (M) upturn, the flow resistance falls.
2. The flow resistance of Au-blood is higher than that of pure blood because gold increases the elasticity of arteries.
3. The stenosis height, angle of proclivity, volume flow rate, Grashof number, heat absorption constraint, and force field constraint all cause an increase in the wall shear stress.
4. A higher absorption constraint and Grashof number cause the fluid's velocity to increase, whereas a higher stenosis height, forced field constraint, and angle of proclivity for it to decrease.
5. Compared to Au-blood, the fluid's velocity is higher for all limitations in the case of pure blood.
6. High buoyancy and electromagnetic forces relative to viscous forces cause the fluid's speed to decrease.
7. The fluid's temperature rises when the heat absorption constraint is increased, but it falls when the stenosis height grows. The tube's center has the highest temperature, while the areas closest to the walls have the lowest.

The results obtained from this study may help medical practitioners to predict the flow behavior in diseased arteries. It also helps control, monitor, and regulate critical blood flow constraints with suitable treatment modalities. There is a scope to discuss the influence of the height of multiple stenoses on resistive impedance, wall shear stress, and in the region between the multiple stenoses.

Ethics declaration

Not Applicable.

CRediT authorship contribution statement

M. Dhange: Conceptualization, Methodology, Software, Validation, Formal analysis, Writing – original draft, Writing – review & editing. **S. Salgare:** Methodology, Software, Writing – review & editing. **Kusal K. Das:** Conceptualization, Software, Formal analysis, Writing – original draft, Writing – review & editing. **Ebenezer Bonyah:** Methodology, Validation, Formal analysis, Writing – original draft, Writing – review & editing. **Habtu Alemayehu:** Conceptualization, Validation, Formal analysis, Writing – original draft, Writing – review & editing.

Declaration of competing interest

The authors declare that they have no known competing financial interests or personal relationships that could have appeared to influence the work reported in this paper.

Acknowledgements

This work was supported by BLDE University grant number BLDEU/ R&D/RGC/2022-23/3329/1. The authors express gratitude for the financial support extended by the BLDE University, India. They also wish to express their gratitude to the very competent anonymous referees for their valuable comments and suggestions.

Data availability

No datasets were generated or analyzed during the current study.

References

[1] D.F. Young, Effect of a time dependent stenosis of flow through a tube, J. Eng. Indust. Trans. ASME. 90 (1968) 248–254.
[2] T. Azuma, T. Fukushima, Flow patterns in stenotic blood vessel models, Biorheol 13 (1976) 337–355.
[3] D.A. Macdonald, On steady flow through modelled vascular stenosis, J. Biomech. 12 (1979) 13–30.
[4] J.H. Forrester, D.F. Young, Flow through a conversing diverging tube and its implications in occlusive vascular disease, J. Biomech. 3 (1970) 297–316.
[5] J.B. Shukla, R.S. Parihar, B.R.P. Rao, Effects of stenosis on non-Newtonian flow through an artery with mild stenosis, Bull. Math. Biol. 42 (1980) 283–294.
[6] J. Perkkio, R. Keskinen, On the effect of the concentration profile of red cells on blood flow in the artery with stenosis, Bull. Math. Biol. 45 (2) (1983) 259–267.
[7] J.C. Misra JC, B.K. Kar, Momentum integral method for studying flow characteristics of blood through a stenosed vessel, Biorheol 26 (1989) 23–35.
[8] P.N. Tandon, U.V. Rana, M. Kawahara, V.K. Katiyar, A model for blood flow through stenotic tube, Int. J. Biomed. Comput. 32 (1993) 62–78.
[9] D.S. Srinivasacharya, D. Srikanth, Effect of couple stresses on the flow in a constricted annulus, Arch. Appl. Mech. 78 (2008) 251–257.
[10] M. Nakamura, T. Sawada, Numerical study on the flow of a non-Newtonian fluid through an axisymmetric stenosis, J. Biomech. Eng. 110 (1988) 137–143.
[11] M.K. Sharma, P.R. Sharma, V. Nasha, Pulsatile MHD arterial blood flow in the presence of double stenosis, J. Appl. Fluid Mech. 6 (3) (2003) 331–338.
[12] N. Verma, R.S. Parihar, Effect of magneto-hydrodynamics and haematocrit on blood flow in an artery with multiple mild stenosis, Int. J. Appl. Math. Comput. 1 (1) (2009) 30–46.
[13] S. Chakravarty, T.K. Mandal, Mathematical modelling of blood flow through an overlapping stenosis, Math. Comput. Model. 19 (1994) 59–73.
[14] S. Chakravarty, T.K. Mandal, A nonlinear two-dimensional model of blood flow in an overlapping arterial stenosis subjected to body acceleration, Math. Comput. Model. 24 (1) (1996) 43–58, https://doi.org/10.1016/0895-7177(96)00079-9.
[15] V.P. Srivastava, S. Mishra, R. Rastogi, Non-Newtonian arterial blood flow through an overlapping stenosis, *Appl. Appl. Math.* Int. J. 5 (1) (2010) 225–238.
[16] V.P. Srivastava, R. Vishnoi, S. Mishra, P. Sinha, A two-layered non-Newtonian arterial blood flow through an overlapping constriction, Appl. Appl. Math. Int. J. 6 (11) (2011) 1781–1797.
[17] D.N. Riahi, R. Roy, S. Cavazos, On arterial blood flow in the presence of an overlapping stenosis, Math. Comput. Model. 54 (2011) 2999–3006, https://doi.org/10.1016/j.mcm.2011.07.028.

[18] A.R. Haghighi, M.A. Shahbazi, Mathematical modeling of micropolar fluid flow through an overlapping arterial stenosis, Int. J. Biomath. 8 (4) (2015) 1550056, https://doi.org/10.1142/S1793524515500564.
[19] J.V.R. Reddy, D. Srikanth, The polar fluid model for blood flow through a tapered artery with overlapping stenosis: effects of catheter and velocity slip, Appl. Bionics Biomech. 15 (2015) 174387, https://doi.org/10.1155/2015/174387.
[20] A. Zaman, N. Ali, O.A. Beg, Unsteady magnetohydrodynamic blood flow in a porous-saturated overlapping stenotic artery: num. model, J. Mech. Med. Biol. 16 (4) (2016) 1650049, https://doi.org/10.1142/S0219519416500494.
[21] M.K. Sharma, V. Nasha, P.R. Sharma, A study for analyzing the effect of overlapping stenosis and dilatation on non-Newtonian blood flow in an inclined artery, J. Biomed. Sci. Eng. 9 (2016) 576–596, https://doi.org/10.4236/jbise.2016.912050.
[22] N.M. Zain, Z. Ismail, Modelling of Newtonian blood flow through a bifurcated artery with the presence of an overlapping stenosis, Mal. J. Fund. Appl. Sci. 1 (2017) 304–309, https://doi.org/10.11113/mjfas.v13n4-1.866.
[23] S. Nadeem, S. Ijaz, Nanoparticles analysis on the blood flow through a tapered catheterized elastic artery with overlapping stenosis, Eur. Phys. J. Plus. 129 (2014) 249, https://doi.org/10.1140/epjp/i2014-14249-1.
[24] S.U.S. Choi, J.A. Eastman, Enhancing thermal conductivity of fluids with nanofluids, ASME Fluids Eng. Div. 231 (1995) 99–105.
[25] J. Buongiorno, Convective transport in nanofluids, J. Heat Trans. 128 (3) (2006) 240–250, https://doi.org/10.1115/1.2150834.
[26] G. Sankad, M. Dhange, Effect of chemical reactions on dispersion of a solute in peristaltic motion of newtonian fluid with wall properties, Malaysian J. Math. Sci. 11 (3) (2017) 347–363.
[27] T. Muhammad, F. Haider, Time dependent flow of Reiner-Rivlin nanofluid over a stretching sheet with Arrhenius activation energy and binary chemical reaction, Multidiscip. Model. Mater. Struct. (2024), https://doi.org/10.1108/mmms-05-2024-0123.
[28] I. Muhammad, T. Muhammad, Numerical simultation of bio-convection radiative heat transport flow of MHD Carreau nanofluid, J. Appl. Mat. Mech. (2024), https://doi.org/10.1002/zamm.202300813.
[29] G.K. Batchelor, The effect of brownian motion on the bulk stress in a suspension of spherical particles, J. Fluid Mech. 83 (1) (1977) 97–117.
[30] Z. Hussain, T. Muhammad, Simultaneous influence of Hall and wall characteristics in peristaltic convective carbon-water flow subject to Soret and Dufour effects, Arabian J. Sci. Eng. 46 (2021) 2033–2046.
[31] M.J. Hatami Hatami, D.D. Ganji, Computer simulation of MHD blood conveying gold nanoparticles as a third grade non-Newtonian nanofluid in a hollow porous vessel, Comput. Meth. Prog. Bio. 113 (2) (2014) 632–641.
[32] K.S. Mekheimer, E.L. EL Elnaqeeb, T.M.A Kot, F. Alghamdi, Simultaneous effect of magnetic field and metallic nanoparticles on a micropolar fluid through an overlapping stenotic artery: blood flow model, Phys. Essays 29 (2) (2016) 272–283, https://doi.org/10.4006/0836-1398-29.2.272.
[33] J.V. Ramana Reddy, D. Srikant, Impact of blood vessel wall flexibility on the temperature and concentration dispersion, J. Appl. Comput. Mech. 6 (3) (2020) 564–581.
[34] A. Safia, M. Zafar, S. Nadeem, Peristaltic transport of a Jeffrey fluid with double diffusive convection in nanofluids in the presence of inclined magnetic field, Int. J. Geom. Methods Mod. Phys. 15 (11) (2018) 1850181, https://doi.org/10.1142/S0219887818501815.
[35] B. Godin, J.H. Sakamoto, R.E. Serda, A. Grattoni, A. Bouamrani, M. Ferrari, Emerging of nano-medicine for the diagnosis and treatment of cardio-vascular diseases, trends, Pharmacol. Sci. 31 (2010) 199–205.
[36] K. Vajravelu, K.V. Prasad, J. Lee, C. Lee, I. Pop, R.A.V. Gorder, Convective heat transfer in the flow of viscous Ag-water and Cu-water nanofluids over a stretching surface, Int. J. Therm. Sci. 50 (2011) 843.
[37] N.S. Akbar, M. Raza, R. Ellahi, Influence of heat generation and heat flux in peristalsis with interaction of nanoparticles, Eur. Phys. J. Plus 129 (2014) 185.
[38] N.S. Akbar, Endoscope effects on the peristaltic flow of Cu-water nanofluids, J. Comut. Theor. Nanosci. 11 (2014) 1150–1155.
[39] N.S. Akbar, E.N. Maraj, A.W. Butt, Copper nanoparticles impinging on a curved channel with complaint walls and peristalsis, Eur. Phys. J. Plus 129 (2014) 183, https://doi.org/10.1140/EPJP/2014-14183-2.
[40] T. Elnaqeeb, K.S. Mekheimer, F. Alghamdi, Cu-blood flow model through a catheterized mild stenotic artery with a thrombosis, Math. Biosci. 282 (2016) 135–146.
[41] A. Zaman, N. Ali, I. Ali, Effects of nanoparticles (Cu, Ag) and slip on unsteady blood flow through a curved stenosed channel with aneurysm, Thermal. Sci. Eng. Prog. 5 (2018) 482–491.
[42] A. Zaman, A.A. Khan, N. Ali, Modelling of unsteady non-Newtonian blood flow through a stenosed artery: with nanoparticles, J. Brazilian Soc. Mech. Sci. Eng. 40 (307) (2018) 1–12, https://doi.org/10.1007/s40430-018-1230-5.
[43] T. Elnaqeeb, N.A. Shah, K.S. Mekheimer, Hemodynamic characteristic of gold nanoparticle blood flow through a tapered stenosed vessel with variable nanofluid viscosity, Bio. *Nano. Sci.* 9 (2019) 245–255, https://doi.org/10.1007/s12668-018-0593-5.
[44] K.S. Mekheimer, T. Elnaqeeb, M.A. ElKot, F. Alghamdi, Simultaneous effect of magnetic filed and metallic nanoparticles on a micropolar fluid through an overlapping stenotic artery: blood flow model, Phy. Essays 29 (2) (2016) 272–283.
[45] J.V.R. Reddy, D. Srikanth, D. Samir, K. Das, Modelling and simulation of temperature and concentration dispersion in a couple stress nanofluid flow through stenotic tapered arteries, Eur. Phys. J. Plus. 132 (8) (2017) 365.
[46] S. Nadeem, S. Ijaz, Nanoparticles analysis on the blood flow through a tapered catheterized elastic artery with overlapping stenosis, Eur. Phys. J. Plus. 129 (11) (2014) 249.
[47] C. Umadevi, M. Dhange, B. Haritha, T. Sudha, Flow of blood mixed with copper nanoparticles in an inclined overlying stenosed artery with magnetic field. *Case stud*, Therm. Eng. 25 (2021) 100947, https://doi.org/10.1016/j.csite.2021.100947.
[48] N.S. Akbar, A.W. Butt, Magnetic field effects for copper suspended nanofluid venture through a composite stenosed arteries with permeable walls, J. Magn. Magn. Mater. 381 (2015) 285–291, https://doi.org/10.1016/j.jmmm.2014.12.084.
[49] A. Zaman, N. Ali, Naneela Kousar, Nanoparticles (Cu, TiO_2, $Al2O_3$) analysis on unsteady blood flow through an artery with a combination of stenosis and aneurysm, Compt. Math. Appl. 76 (9) (2018) 2179–2191, https://doi.org/10.1016/j.camwa.2018.08.019.
[50] N.S. Akbar, M.T. Mustafa, Ferromagnetic effects for nanofluid venture through composite permeable stenosed arteries with different nanosize particles, AIP Adv. 5 (2015) 077102, https://doi.org/10.1063/1.4926342.
[51] N.S. Akbar, Metalic nanoparticle analysis for the blood flow in tapered stenosed arteries: application in nanomedicines, Int. J. Bio. Math. 9 (1) (2016) 1–18, https://doi.org/10.1142/S1793524516500029.
[52] B.C. Pak, Y.I. Cho, Hydrodynamic and heat transfer study of dispersed fluids with submicron metallic oxide particles, Exp. Heat Transf. 11 (2) (1998) 151–170.
[53] K.S. Mekheimer, M.S. Mohamed, T. Elnaqeeb, Metallic nanoparticles influence on blood flow through a stenotic artery, Int. J. Pure. Appl. Math. 107 (1) (2016) 201–220.
[54] T. Elnaqeeb, Modeling of Au (NPs)-blood flow through a catheterized multiple stenosed artery under radial magnetic field, Eur. Phys. J. 228 (2019) 2695–2712, https://doi.org/10.1140/epjst/e2019-900059-9.
[55] Y. Pratumwal, W. Limtrakaran, S. Muengtaweepongsa, P. Phakdeesan, K. Intharakham, Whole blood viscosity modelling using power las, Casson, and Carreau Yasuda models interegrated with image scanning U-tube viscometer technique, Songklanakarin J. Sci. Technol. 39 (5) (2017) 625–631.
[56] R. Sardar, A.M. Funston, P. Mulvaney, et al., Gold nanoparticles: past, present, and future, Langmuir 25 (24) (2009) 13840–13851.
[57] L.H. Madkour, Applications of gold nanoparticles in medicine and therapy, Pharm. *Pharmacol. Int. J.* 6 (3) (2018) 157–174.
[58] P.S. Mwita, N. Shaban, I. Mbalawata, M. Mayige, Mathematical modeling of root causes of hyperglycemia and hypoglycemia in a diabetes mellitus patient, Sci. African. 14 (2021) e0142.
[59] N. Abae Ange-Boris, Y. Pavel, M.K. Edoukoua Jean, A.K. Michel, T.J. Zoueu, Characterization of red blood cells infected by plasmodium falciparum using optical tweezes, Sci. African. 27 (2025) e02553.
[60] N.S. Akbar, T. Muhammad, Physical aspect of electro osmotically interactive cilia propulsion on symmetric plus asymmetric conduit flow of couple stress fluid with thermal radiation and heat transfer, Sci. Rep. 13 (2023) 18491.